Smart Mater. Struct. **22** (2013) 085015 (12pp) doi:10.1088/0964-1726/22/8/085015

Nonlinear dynamic modeling and resonance tuning of Galfenol vibration absorbers

Justin J Scheidler and Marcelo J Dapino

Smart Materials and Structures Lab, Smart Vehicle Concepts Center, Department of Mechanical and Aerospace Engineering, The Ohio State University, Columbus, OH 43210, USA

E-mail: scheidler.8@osu.edu and dapino.1@osu.edu

Received 9 May 2013, in final form 13 May 2013
Published 11 July 2013
Online at stacks.iop.org/SMS/22/085015

Abstract
This paper investigates the semi-active control of a magnetically-tunable vibration absorber's resonance frequency. The vibration absorber that is considered is a metal-matrix composite containing the magnetostrictive material Galfenol (FeGa). A single degree of freedom model for the nonlinear vibration of the absorber is presented. The model is valid under arbitrary stress and magnetic field, and incorporates the variation in Galfenol's elastic modulus throughout the composite as well as Galfenol's asymmetric tension–compression behavior. Two boundary conditions—cantilevered and clamped–clamped—are imposed on the composite. The frequency response of the absorber to harmonic base excitation is calculated as a function of the operating conditions to determine the composite's capacity for resonance tuning. The results show that nearly uniform controllability of the vibration absorber's resonance frequency is possible below a threshold of the input power amplitude using weak magnetic fields of 0–8 kA m^{-1}. Parametric studies are presented to characterize the effect on resonance tunability of Galfenol volume fraction and Galfenol location within the composite. The applicability of the results to composites of varying geometry and containing different Galfenol materials is discussed.

(Some figures may appear in colour only in the online journal)

1. Introduction

The incorporation of smart materials into control systems can improve semi-active and active vibration control design. The optimal smart material for a specific vibration control system depends upon the operating conditions in service and the performance requirements. For applications in which the smart material is subject to appreciable stress, most smart materials cannot be utilized, because only a few can withstand tensile and shear loading or operate in harsh mechanical environments. Shape memory alloys are robust, but their bandwidth is limited to $\mathcal{O}(1)$ Hz due to their thermal activation, and provide very limited sensing capabilities [1]. One attractive smart material for high stress applications is iron–gallium (Galfenol, $Fe_{100-x}Ga_x$).

Galfenol's structural-grade tensile strength (∼500 MPa) [2], ability to withstand torsion and impact, frequency bandwidth on the order of 10 kHz, ability to be magnetized easily, and very low hysteresis are beneficial for active vibration reduction systems. This combination of properties is not found in any other smart material. The main drawbacks of Galfenol are its moderate magnetostriction (350×10^{-6} to 400×10^{-6} for single crystals) [2, 3] and its relatively low energy density (∼3 kJ m^{-3}) [4], which is about 10 times less than that of Terfenol-D (25 kJ m^{-3}) [5] and piezoceramics (∼31 kJ m^{-3}) [6]. This limited work output hinders active vibration control implementation. As such, semi-active vibration reduction is considered in this paper.

Galfenol's suitability for semi-active control derives from the Delta E (ΔE) effect,

$$\Delta E = (E(H, T) - E_0)/E_0, \tag{1}$$

where $E(H, T)$ is the elastic modulus at magnetic field H and stress T, and $E_0 = E(0, 0)$. This definition is adapted

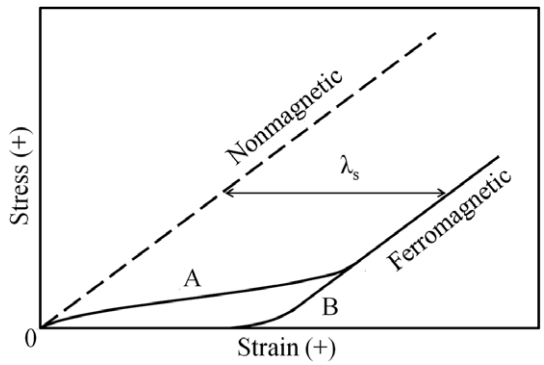

Figure 1. Stress versus strain for (A) initially demagnetized and (B) initially partially magnetized ferromagnetic materials with positive maximum magnetostriction λ_s.

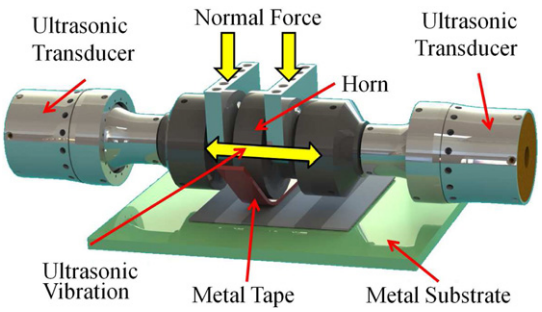

Figure 2. Schematic of the UAM process.

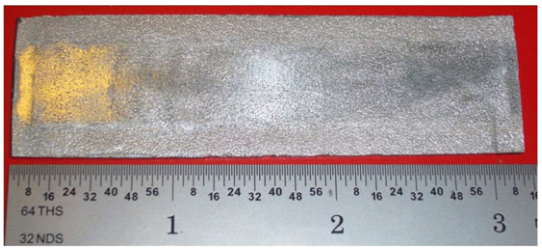

Figure 3. Al 3003 composite manufactured by UAM containing an embedded 0.05 cm × 1.27 cm × 7.62 cm Galfenol sheet.

from Bozorth [7], and is a generalization of that presented by Flatau *et al* [8]. The ΔE effect is illustrated in figure 1. When Galfenol is mechanically loaded from a state of zero stress and magnetization (shown by path A in figure 1), both purely mechanical and magnetoelastic strain occur until the material becomes magnetically saturated, after which only purely mechanical strain occurs. Thus, Galfenol's effective elastic modulus varies while its magnetic state changes.

Since Galfenol has structural strength, it can be located in the load path. Methods for incorporating Galfenol into load-carrying structures are needed. A powerful technique for seamlessly embedding smart materials into metal matrices is ultrasonic additive manufacturing (UAM), also known as ultrasonic consolidation. UAM is a new rapid prototyping process for creating solid-state, metallurgical welding at the interface between a thin metallic tape and a metallic substrate. This is accomplished by applying a static, normal compressive force between a cylindrical welding horn and the tape–substrate pair while vibrating the horn laterally at ultrasonic frequencies, as shown in figure 2. Like all solid-state welding processes, metallurgical welding occurs below the melting temperatures of the respective metals—roughly 35% of the melting temperature for UAM [9]. UAM therefore provides the unique ability to either weld or encapsulate smart materials, electronics, and fiber optics inside a metal matrix. A Galfenol-Al 3003 composite manufactured via UAM is shown in figure 3.

System-level modeling of magnetostrictive-based structures in relation to vibration control has been documented. Mudivarthi *et al* [10] presented a 3D finite element model to calculate the bidirectionally coupled magnetoelastic response of a Galfenol unimorph sensor, including the ΔE effect. The model is static and did not consider the asymmetry in Galfenol's tension–compression behavior. Braghin *et al* [11] developed a 1D model of uniaxial, magnetostrictive-based actuators using a linear model of the Terfenol-D behavior. Although the model is claimed to be valid for an actuation bandwidth of 2 kHz, its scope is restricted to operation in linear constitutive regimes and for negligible eddy currents. Shu *et al* [12] developed a 1D dynamic model of a Galfenol unimorph by coupling Euler–Bernoulli beam theory with a linear constitutive model of Galfenol. In addition to the linearity assumption on Galfenol's behavior, this model did not consider the effect of stress on the magnetostrictive response. Zhou and Zhou [13] modeled the 1D nonlinear vibration of a carbon fiber reinforced plastic composite containing layers of Terfenol-D particles by coupling Euler–Bernoulli beam theory with a nonlinear constitutive model of Terfenol-D. They quantified the vibration reduction caused by velocity feedback, and investigated the effect of material properties, lamination scheme, and location of Terfenol-D layers. Optimal vibration control occurred when the magnetostrictive layer was located away from the neutral axis of the composite. The ΔE effect was not investigated. Further, the underlying constitutive model for the magnetostrictive material is less accurate than that of Evans and Dapino [14], because it relies on curve fits to experimental data to develop expressions for both magnetostriction and magnetization. Scheidler and Dapino [15] modeled the 1D nonlinear vibration of a Galfenol-based metal-matrix composite under cantilevered boundary conditions. Frequency responses were approximated to investigate the tunability of the composite's resonance through control of the bias magnetic field. The expression used to calculate the strain in the Galfenol element is applicable to axial vibration, but not bending vibration. The asymmetry in Galfenol's tension–compression behavior and the variation in the material's elastic modulus along the length of the beam were not considered.

In this paper, a metal-matrix composite, like that shown in figure 3, containing an embedded sheet of Galfenol is considered. The objective of the paper is to assess the controllability of the composite's resonance through bias field tuning of Galfenol's elastic modulus. The

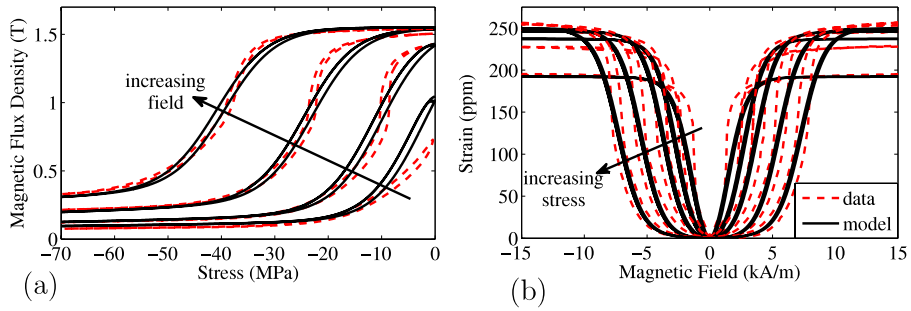

Figure 4. Comparison of experimental and calculated (a) sensing and (b) actuation responses (experimental data taken from [14]).

nonlinear bending vibration of the composite is modeled to quantify changes in the composite's frequency response due to variations in the excitation power amplitude and the bias magnetic field. For computational purposes, the composite is approximated as a simple mass–spring–damper system, where the spring behaves nonlinearly due to the stress and magnetic field-dependent elastic modulus of Galfenol. The approach has the following advantages: (i) it incorporates a fully coupled, nonlinear constitutive model of Galfenol that is accurate for arbitrary stress and magnetic field, (ii) it considers the variation in Galfenol's elastic modulus along the length of the composite, and (iii) it includes the asymmetric tension–compression behavior of Galfenol. Two boundary conditions, clamped–free (C–F) and clamped–clamped (C–C), are considered. To optimize the composite geometry for resonance tuning, a parametric study is presented to determine the effect of Galfenol volume fraction and of the location of Galfenol elements within the composite.

2. Model development

The frequency domain response of the composite's vibration is desired to quantify the tunability of the composite's resonance. However, an eigenvalue problem cannot be formulated for it, because the composite's stiffness nonlinearity is state dependent. Consequently, the frequency response must be approximated by calculating the steady-state vibration in the time domain and extracting the vibration amplitudes at discrete excitation frequencies. The number of time domain responses required to approximate the frequency responses for the parametric studies is $\mathcal{O}(10^4)$, because (i) ∼30 discrete frequencies are needed for smoothness of the frequency responses, (ii) both forward and reverse frequency sweeps are required, (iii) a wide range of operating conditions (excitation power amplitude and bias magnetic field) must be considered, and (iv) the independent parameter (Galfenol volume fraction or location) must be varied. As such, the system must be simplified for computational efficiency. To preserve the complex constitutive behavior of Galfenol, the composite is approximated as a single lumped mass with an equivalent bending stiffness and constant damping.

2.1. Galfenol constitutive model

Due to the nonlinearities of magnetostrictive materials, namely magnetic saturation, magnetic anisotropy, and a nearly quadratic magnetostriction dependence on magnetization, linear models are accurate only for small amplitude operation about a bias point. To describe the full-scale Galfenol behavior, the 1D anhysteretic formulation of the efficient, fully coupled Evans–Dapino (ED) model [14, 16] is used. This model has been successfully used to quantify the 3D nonlinear dynamic actuation of a Galfenol unimorph [17, 18] and the major and minor stress-magnetization loops of a Galfenol rod [19, 20].

The ED model calculates Galfenol's magnetization and strain as functions of magnetic field $\mathbf{H} = (H_1, H_2, H_3)^{\mathrm{T}}$ and stress $\mathbf{T} = (T_1, T_2, T_3, T_4, T_5, T_6)^{\mathrm{T}}$. The ED model is summarized below, and a condensed derivation is shown in the appendix. Energy functions accounting for magnetoelastic, applied magnetic field, and crystalline anisotropy contributions are locally defined about each of the easy crystallographic directions. The orientation of each preferred magnetization direction in response to applied stresses and magnetic fields is then calculated through energy minimization. The volume fraction of magnetic domains oriented in each of the preferred directions is then calculated by an energy-weighted average so that lower energy directions are favored. Finally, the macroscopic magnetization and strain are calculated as the sum of the contribution from each orientation weighted by the volume fraction of domains in each orientation. The accuracy of the model is illustrated in figure 4, where a comparison to experimental measurements of a ⟨100⟩ textured $Fe_{81.5}Ga_{18.5}$ rod is shown. The ED model can also be analytically differentiated to provide expressions for the elastic modulus of Galfenol, which is shown in figure 5 as a function of stress and magnetic field.

2.2. Bending vibration model

Following the standard application of Newton's second law, the governing ODE for the composite beam represented as a single degree of freedom resonator is

$$m\ddot{u} + c\dot{u} + K_{\mathrm{eq}}(H_{\mathrm{bias}}, T)u = m\omega^2 U_2 \mathrm{e}^{\mathrm{i}\omega t}, \qquad (2)$$

where u is defined as the relative displacement between mass and base, and harmonic base excitation with amplitude U_2 and

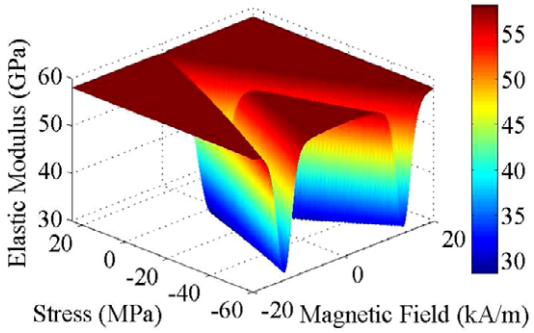

Figure 5. Variation in Galfenol's linear elastic modulus calculated using the ED model.

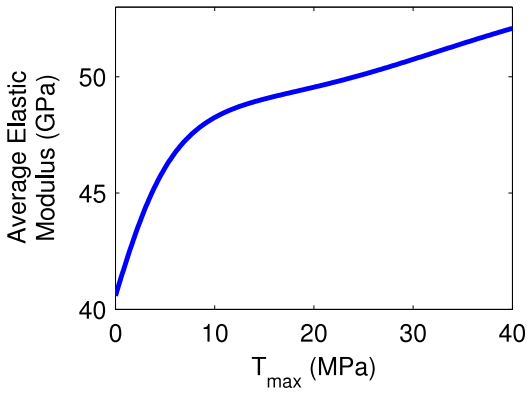

Figure 6. Average elastic modulus through the thickness of a Galfenol element located at the neutral axis with $H_{\text{bias}} = 2$ kA m^{-1} (calculated using the ED model).

frequency ω is used,

$$u = u_1 - u_2 = u_1 - U_2 e^{i\omega t}. \tag{3}$$

In (2) the spring is nonlinear due to the dependence of Galfenol's elastic modulus on the bias magnetic field (H_{bias}) and bending stress (T). The magnetic field is assumed homogenous throughout the composite. The damping ratio,

$$\xi = \frac{c}{2m\omega_n} = \frac{c}{2m}\sqrt{\frac{m}{K_{\text{eq}}}}, \tag{4}$$

was held constant for all simulations. Using results from Meirovitch [21], the equivalent spring constants for a C–F beam subject to a tip load and a C–C beam subject to midspan load are

$$K_{\text{eq}}^{\text{CF}}(H_{\text{bias}}, T) = \frac{3E_{\text{eq}}(H_{\text{bias}}, T)I(H_{\text{bias}}, T)}{L^3} \tag{5}$$

and

$$K_{\text{eq}}^{\text{CC}}(H_{\text{bias}}, T) = \frac{192E_{\text{eq}}(H_{\text{bias}}, T)I(H_{\text{bias}}, T)}{L^3}, \tag{6}$$

respectively, where L is the length of the beam. As such, u represents the tip deflection of the C–F beam and the midspan deflection of the C–C beam. The equivalent elastic modulus of the composite E_{eq} is calculated as a function of the matrix and average Galfenol elastic moduli (E_{M} and E_{G}) and volume fractions (ξ_{M} and ξ_{G}) using the rule of mixtures [22],

$$E_{\text{eq}}(H_{\text{bias}}, T) = E_{\text{G}}(H_{\text{bias}}, T)\xi_{\text{G}} + E_{\text{M}}\xi_{\text{M}}. \tag{7}$$

The area moment of inertia I is calculated in the standard manner after first homogenizing the composite by scaling the Galfenol width (W_{G}) to yield an equivalent section of matrix material,

$$W_{\text{G}_{\text{eq}}} = \frac{E_{\text{G}}(H_{\text{bias}}, T)}{E_{\text{M}}} W_{\text{G}}. \tag{8}$$

Considering the stress variation in the beam and the asymmetry in the material's tension–compression behavior, an average elastic modulus for the Galfenol element is calculated. As seen in figures 4(a) and 5, respectively, the magnetic flux in Galfenol and its elastic modulus vary almost exclusively in the compressive stress regime. Thus, even for Galfenol located at the neutral axis, the symmetric (zero average) bending stress will yield an asymmetric elastic modulus distribution through the Galfenol thickness. This asymmetric distribution will change as the stress magnitude varies, leading to a non-constant average elastic modulus through the Galfenol element's thickness. An example of this variation in elastic modulus is shown in figure 6 as a function of the maximum bending stress in a Galfenol beam.

Galfenol's elastic modulus varies along the length of the beam due to the position-dependent stress in the Galfenol element. This variation is incorporated in the single degree of freedom model of the composite by using an average value of the stress in the element. As will be discussed in section 3, the stress acting on the Galfenol element is calculated from its strain using a numerical inversion of the ED model. Thus, an average value of the strain is required.

The strain in the Galfenol element at a distance y from the neutral axis is calculated from mechanics of materials as

$$S = -y\frac{\partial^2 w}{\partial x^2}, \tag{9}$$

where $w(x)$ is the transverse deflection of the beam along its length. This strain is evaluated at each time step by assuming that the instantaneous beam deflection is due to a virtual, static force F at the tip (for the C–F beam) or the midspan (for the C–C beam). Under these conditions, the elastic curves of the C–F and C–C beams are

$$w^{\text{CF}}(x) = \frac{1}{2E_{\text{eq}}I}\left(FLx^2 - \frac{1}{3}Fx^3\right) \tag{10}$$

and

$$w^{\text{CC}}(x) = \begin{cases} (4E_{\text{eq}}I)^{-1}\left(-\frac{1}{3}Fx^3 + \frac{1}{4}FLx^2\right) \\ \qquad 0 \le x \le \dfrac{L}{2} \\ (4E_{\text{eq}}I)^{-1}\left(\frac{1}{3}Fx^3 - \frac{3}{4}FLx^2 + \frac{1}{2}FL^2x - \frac{1}{12}FL^3\right) \\ \qquad \dfrac{L}{2} \le x \le L, \end{cases} \tag{11}$$

respectively. The average curvature of the C–F beam is

$$\left(\frac{\partial^2 w}{\partial x^2}\right)_{\text{avg}}^{\text{CF}} = \frac{FL}{2E_{\text{eq}}I}. \tag{12}$$

Setting $x = L$ in (10) to relate the calculated tip deflection u^{CF} to the virtual tip force and using (12), the strain in the Galfenol element (9) for the C–F beam can be rewritten as

$$S^{\text{CF}} = -\frac{3u^{\text{CF}}y}{2L^2}. \tag{13}$$

For the C–C beam, the average curvature is zero. Despite this, the average elastic modulus of the Galfenol element will still vary even if it is also located at the beam's neutral axis. For the C–C beam, the average curvature over the middle half and over the outer quarters of the beam,

$$\left(\frac{\partial^2 w}{\partial x^2}\right)_{\text{avg1}}^{\text{CC}} = \frac{-FL}{16E_{\text{eq}}I} \tag{14}$$

and

$$\left(\frac{\partial^2 w}{\partial x^2}\right)_{\text{avg2}}^{\text{CC}} = \frac{FL}{16E_{\text{eq}}I}, \tag{15}$$

respectively, are both used. Setting $x = L/2$ in (11) to relate the calculated midspan deflection u^{CC} to the virtual midspan force and using (14) and (15), the strain in the Galfenol element (9) over these sections of the C–C beam can be rewritten as

$$S_1^{\text{CC}} = \frac{12u^{\text{CC}}y}{L^2} \tag{16}$$

and

$$S_2^{\text{CC}} = -\frac{12u^{\text{CC}}y}{L^2}. \tag{17}$$

In summary, the change in Galfenol's elastic modulus along the length of the beam is incorporated into the proposed model using a single average strain (13) for the C–F beam and two average strains (16) and (17) for the C–C beam.

The variation in Galfenol's elastic modulus through the element's thickness is considered by averaging the elastic moduli that are calculated at 2, 4, 6, 8, and 10 equally-spaced locations through the thickness. The number of locations necessary for an accurate approximation was determined through a small parametric study. The independent variables in the study were the bias magnetic field (values of 0, 2, and 4 kA m^{-1}) and the location of the Galfenol element (at the neutral axis, 75% of the element above the neutral axis, and 75% of the element below the neutral axis). For each case, the force applied to the beams was varied such that the maximum stress in the Galfenol element varied between 0 and 350 MPa. A uniform grid of points was applied to the Galfenol element (100 points through its thickness and 100 points along its length). At each grid point, the strain was calculated using (9). The true average elastic modulus in the Galfenol element was taken as the average over this 100 × 100 grid. An example comparison between the true average and the approximated averages is shown in figure 7. For each case, the RMS error was calculated relative to the true average. The average RMS error over all of the test cases is tabulated in table 1 for each approximation.

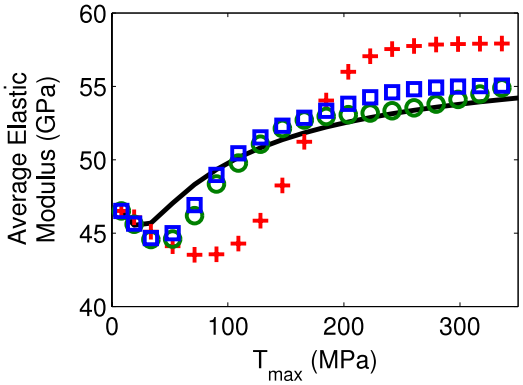

Figure 7. Average elastic modulus of a Galfenol element located at the C–F beam's neutral axis calculated from 2 (+), 6 (○), and 10 (□) locations through the element's thickness compared to the true average (—) ($H_{\text{bias}} = 4$ kA m^{-1}; 4 and 8 location averages not shown for clarity).

Table 1. Average RMS error for approximating the average elastic modulus through the thickness and along the length of the Galfenol element using 2, 4, 6, 8, and 10 equally-spaced locations through its thickness.

	Average RMS error (GPa)	
Number of locations	C–F beam	C–C beam
2	4.06	2.41
4	2.40	1.70
6	1.80	1.49
8	1.80	1.54
10	1.82	1.62

Note that the approximations for the C–C beam average twice as many elastic moduli as for the C–F beam, because two average strains (and therefore two elastic moduli) are needed to describe the elastic modulus variation along the C–C beam's length. Considering accuracy and computational efficiency of the composite's vibration model, 6 and 4 averages through the Galfenol element's thickness were used for the C–F and C–C beams, respectively.

3. Nonlinear solution procedure

The solution procedure is graphically depicted in figure 8. The inner loop approximates the nonlinear time domain response of the composite beam through linearization of the nonlinear ODE (2) by updating the equivalent stiffness for each time step. The ED model is used to update Galfenol's elastic modulus, which requires knowledge of the stress and magnetic field in the Galfenol element. The magnetic field is a known input. However, due to the bidirectional coupling present in the Galfenol element, direct calculation of the stress from the beam deflection is not possible. Instead, stress must be calculated from the bias magnetic field and strain in the Galfenol element by numerically inverting the ED model. In

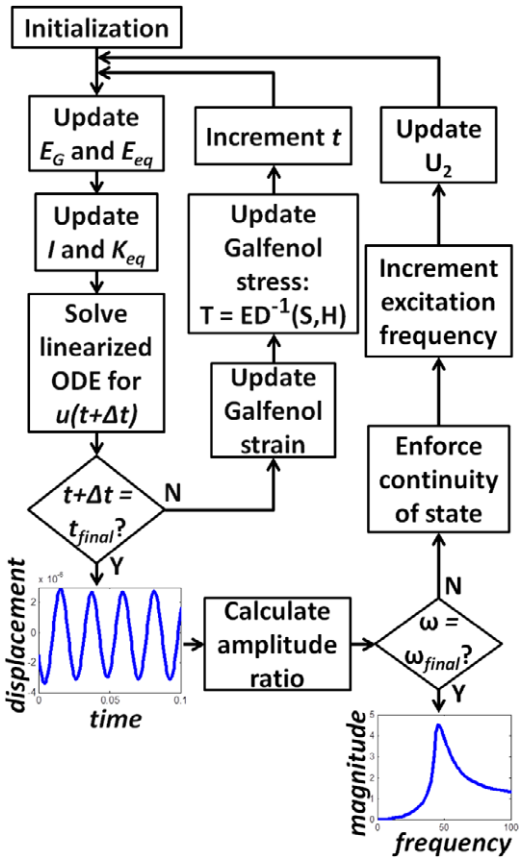

Figure 8. Solution procedure to approximate a single, potentially hysteretic frequency response.

this paper, the inversion is performed using the quasi-Newton SR1 algorithm [17]. Therefore, for each time increment, the strain, stress, and elastic modulus must be calculated at each of the 6 and 8 averaging locations for the C–F and C–C beams, respectively. Each cycle of the excitation is divided into 50 differential time steps to maintain accuracy and smoothness. Solutions are obtained for 15 cycles of the base excitation, which was determined *a posteriori* to ensure that the steady state was reached.

The outer loop approximates the frequency response of the composite's nonlinear vibration. The amplitude ratio is calculated as the steady-state tip or midspan displacement divided by the excitation amplitude. Forward and reverse excitation frequency sweeps are necessary due to the nonlinearities in the system, which may result in multiple, stable periodic orbits of the composite's vibration for a single set of operating conditions. When this occurs, it is seen in the frequency response as hysteresis in the steady-state vibration of the system. This also explains the need for enforcing continuity of state (i.e., equating the initial state of the next time domain response with the final state of the current response) at the beginning of each time domain simulation.

A hysteretic frequency response obtained using the proposed model is shown in figure 9. Throughout each frequency sweep, the input power amplitude $|P| = |Fv|$ is held

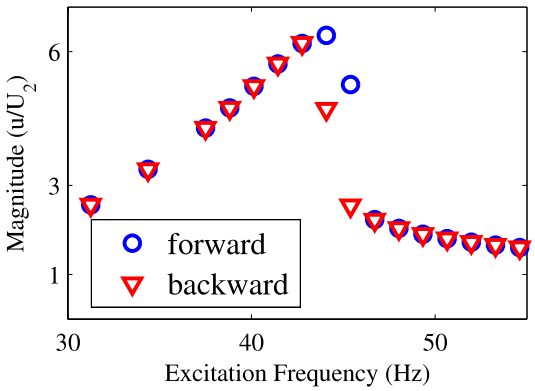

Figure 9. Hysteretic frequency response of the C–F Galfenol-Al composite, $H_{bias} = 1$ kA m^{-1}, $|P| = 0.0119$ J, and $\xi_G = 0.82$.

constant by defining the excitation amplitude as

$$U_2 = \sqrt{\frac{|P|}{m\omega^3}}, \tag{18}$$

which can be derived from (2) and (3). This is a more physically accurate operating condition than that used by Scheidler and Dapino [15]. This numerical simulation is equivalent to a forward and reverse stepped sine experiment that includes the first vibration mode.

4. Model results

The entire range of composite behavior is described by the excitation magnitude and the bias magnetic field. Thus, a complete characterization of the stiffness tuning behavior, and therefore natural frequency tuning behavior, is obtained by considering a range of input power amplitudes (1×10^{-3} to 1×10^{4} J) that leads to Galfenol stresses between 50 and -50 MPa and bias magnetic fields (0 to 13 kA m^{-1}) capable of magnetically saturating the Galfenol element over this stress range. The 1D strain response of Galfenol is symmetric with respect to magnetic field. Therefore, negative bias magnetic fields do not need to be considered. To accurately approximate the natural frequency for each case, both the forward and reverse frequency sweeps were curve fit with cubic splines. The natural frequency was taken as the frequency at which the maximum amplitude ratio occurs in the interpolated data. The natural frequency of vibration for every combination of input power amplitude and bias magnetic field was obtained in this manner. The resulting frequencies were normalized with respect to the maximum frequency to show the percentage changes in resonance frequency from the saturated (stiff) case.

In order to determine the geometry that maximizes the stiffness tunability of the composite, the Galfenol volume fraction and its offset from the horizontal midplane of the composite's cross section were varied. Surface plots of the normalized natural frequency were generated for each case; these plots are presented as a top view of the surface in figures 10, 11, 13, and 14. Results are presented for the model parameters given in table 2; the material properties for Galfenol were obtained through a

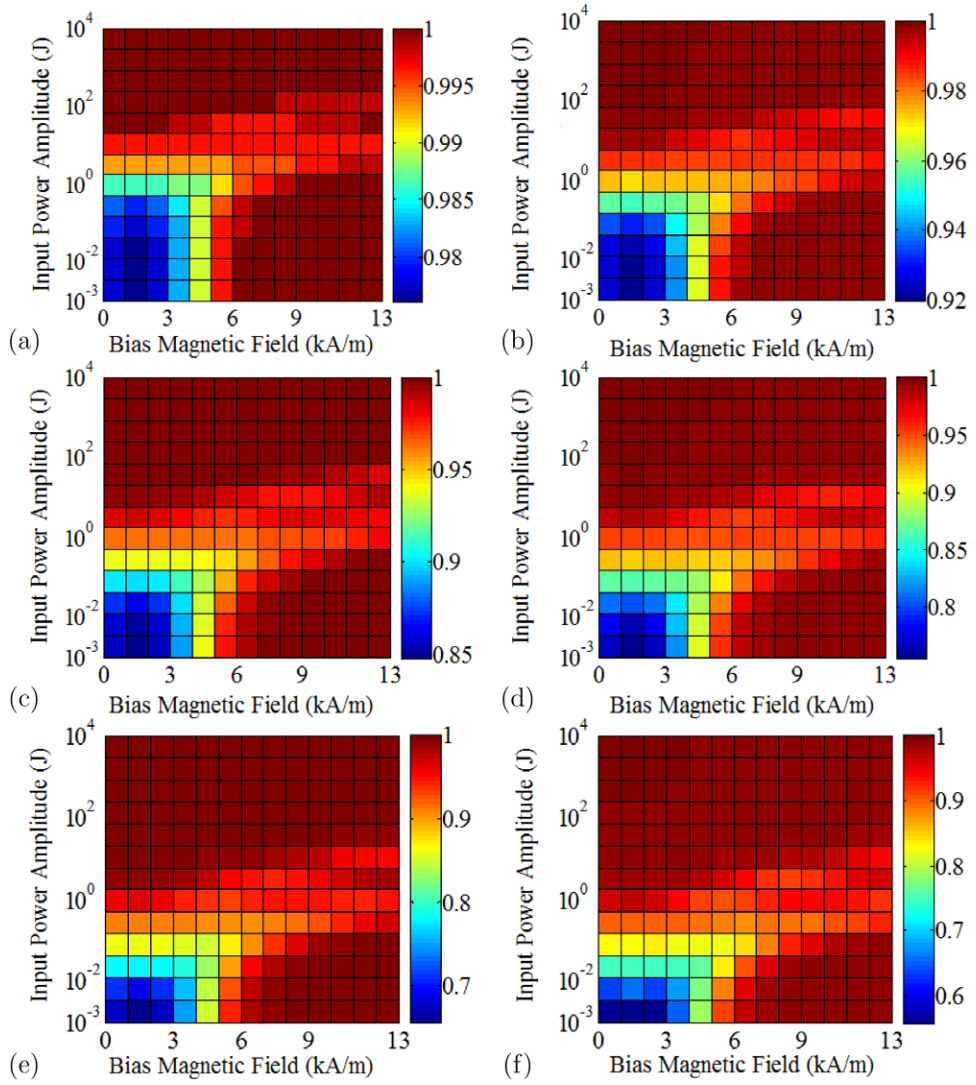

Figure 10. Normalized natural frequency of the C–F composite as a function of the operating conditions for Galfenol volume fractions of (a) 10%, (b) 28%, (c) 46%, (d) 64%, (e) 82%, and (f) 100% (top views shown, Galfenol embedded at the neutral axis). Natural frequencies normalized with respect to the saturated (stiff) case.

Table 2. Model parameters.

FeGa				Matrix (Al)	Composite				
M_s (T)	λ_{100} ($\times 10^{-6}$)	K^k (kJ m^{-3})	Ω (J m^{-3})	E (GPa)	ξ	L (cm)	m (kg)	Width (cm)	Thickness (cm)
1.3787	157	2.71×10^4	776.73	68.9	0.1	2.54	0.058	1.65	0.0762

least squares optimization routine using the anhysteretic ED model and experimental measurements of a highly-textured, polycrystalline $Fe_{81.6}Ga_{18.4}$ Galfenol rod [20].

For the parametric study of Galfenol volume fraction, the Galfenol element was located at the horizontal midplane of the composite's cross section, while its volume fraction was varied between 10% and 100% (i.e., the limiting case of no surrounding matrix). A surface plot of the composite's normalized natural frequency is shown for each case in figures 10 and 11 for the C–F and C–C beams, respectively. The surface plots for negative bias magnetic fields are simply reflections about the $H_{\text{bias}} = 0$ line of those shown in figures 10 and 11. The maximum resonance tunability as a function of the volume fraction is summarized in figure 12.

The parametric study of Galfenol's location was conducted by holding the volume fraction of Galfenol constant at 10%, while varying Galfenol's location vertically in the composite cross section. Four different cases were modeled: (i) the reference case—Galfenol midplane coincident with the composite midplane, (ii) Galfenol midplane shifted upward 33% of the limiting value, (iii) Galfenol midplane shifted upward 66% of the limiting value, and (iv) the limiting case—top surface of Galfenol coincident with the top surface of the composite. A surface plot of

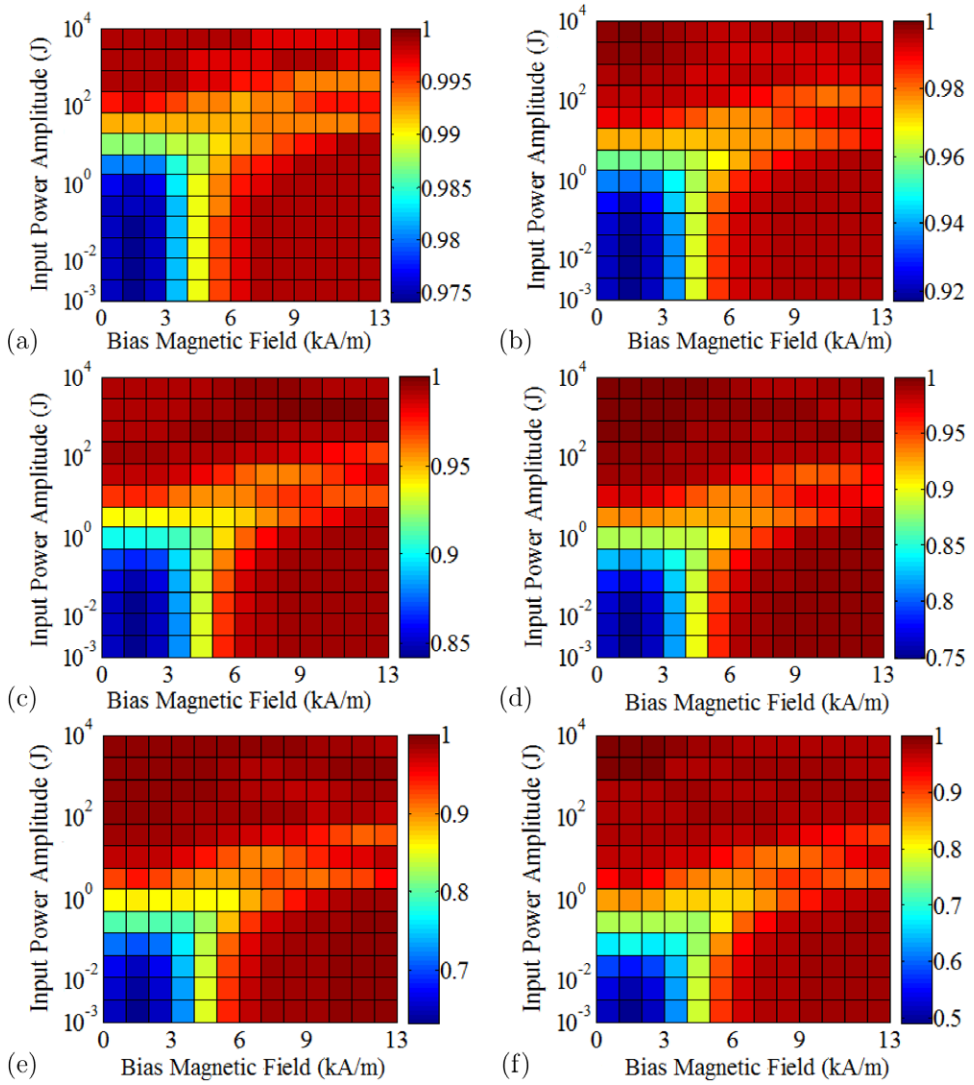

Figure 11. Normalized natural frequency of the C–C composite as a function of the operating conditions for Galfenol volume fractions of (a) 10%, (b) 28%, (c) 46%, (d) 64%, (e) 82%, and (f) 100% (top views shown, Galfenol embedded at the neutral axis).

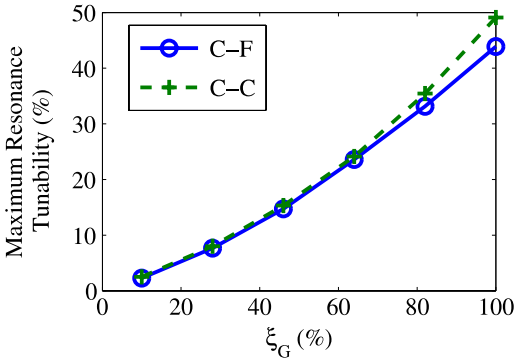

Figure 12. Effect of Galfenol volume fraction on the maximum tunability of the vibration absorber's resonance for C–F and C–C boundary conditions (Galfenol embedded at the neutral axis).

the composite's normalized natural frequency is shown for each case in figures 13 and 14 for the C–F and C–C beams, respectively. The maximum resonance tunability as a function of Galfenol's offset from the composite midplane is summarized in figure 15.

5. Discussion

For a given input power amplitude, semi-active control of the vibration absorber's resonance is accomplished by regulating the composite's resonance between its minimum and maximum frequencies through changes in the bias magnetic field. The results show that nearly uniform controllability occurs below a threshold of the input power amplitude (i.e., $\sim 5 \times 10^{-1}$ J for the C–F boundary conditions, $\xi_G = 0.1$, and Galfenol located at the neutral axis). The maximum tunability of the vibration absorber's resonance also occurs in this region, and can be achieved with relatively weak magnetic fields of 8 kA m^{-1} or less.

Above the threshold of the input power amplitude, the composite's capacity for resonance tuning decreases, and eventually the composite's natural frequency becomes

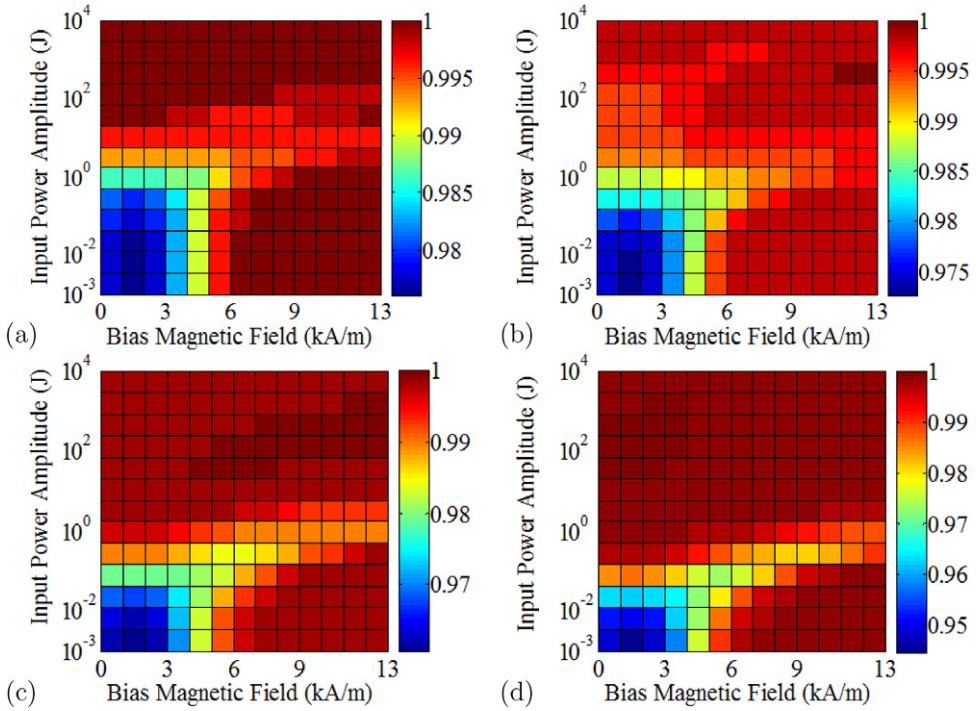

Figure 13. Normalized natural frequency of the C–F composite as a function of the operating conditions for Galfenol embedded at the (a) reference or minimum, (b) 33%, (c) 66%, and (d) 100% or maximum locations (top views shown, $\xi_G = 0.1$).

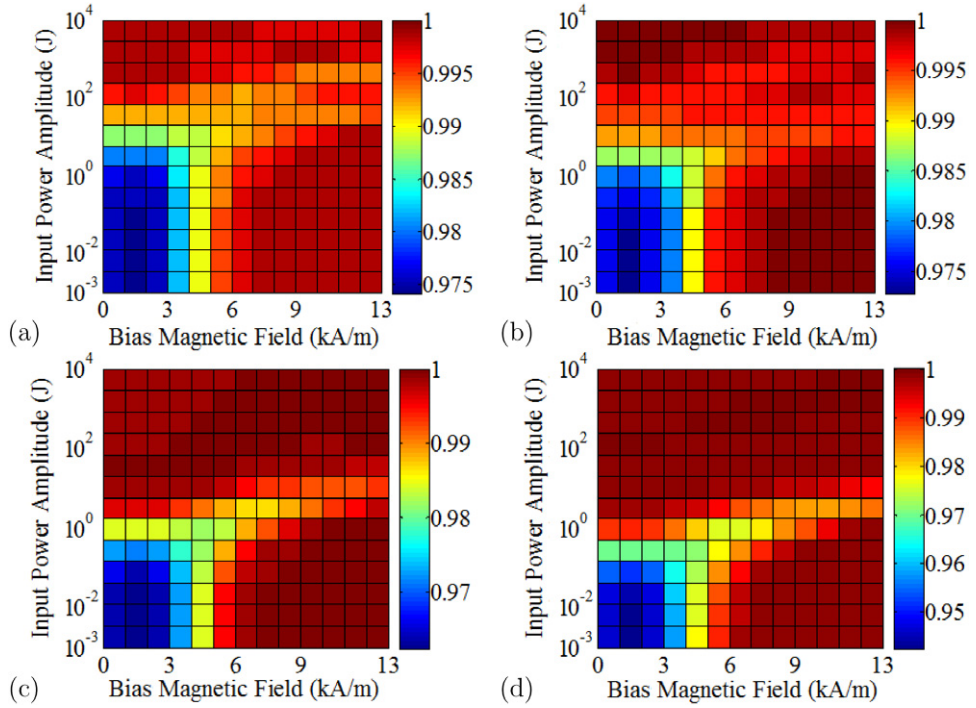

Figure 14. Normalized natural frequency of the C–C composite as a function of the operating conditions for Galfenol embedded at the (a) reference or minimum, (b) 33%, (c) 66%, and (d) 100% or maximum locations (top views shown, $\xi_G = 0.1$).

uncontrollable. Despite this, some controllability exists over a wide range (∼3 to 5 orders of magnitude) of the power amplitude of the excitation. The decrease in controllability is attributed to the increased stress on the Galfenol element as the power amplitude increases. Galfenol becomes magnetically saturated when subject to sufficiently large compressive stresses, causing the elastic modulus to saturate (see figure 5). Thus, the expression,

$$\lim_{|T|\to\infty} E_G(t) = E_G^{\text{saturated}} \approx 58 \text{ GPa}, \tag{19}$$

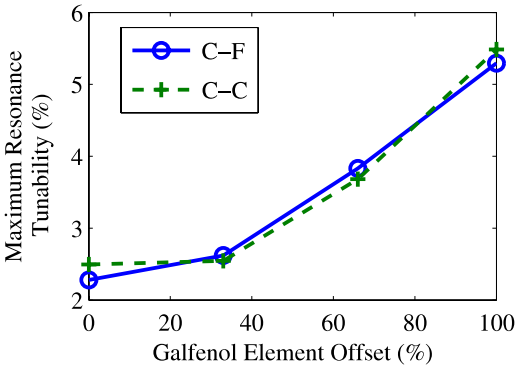

Figure 15. Effect of Galfenol's vertical location in the composite on the maximum tunability of the vibration absorber's resonance for the C–F and C–C boundary conditions ($\xi_G = 0.1$).

holds for 1D Galfenol elements. This tendency toward a constant elastic modulus is slowed by increasing the bias magnetic field to counteract increases in the stress amplitude. This explains why the location of the minimum resonance in figures 10 and 11 shifts to higher magnetic fields as the input power amplitude increases above the threshold value.

From the above reasoning, it can be postulated that the effect of the input power amplitude will depend upon the composite's geometry. The power amplitude threshold will be lower for more compliant composites, and vice versa. This is supported by the results of the parametric studies. As seen in figures 10 and 11, the threshold decreases as Galfenol volume fraction increases, because the aluminum matrix is replaced with a softer material. Similarly in figures 13 and 14, the threshold decreases as Galfenol is shifted away from the neutral axis due to a decrease in the composite's area moment of inertia and an increased bending stress on the Galfenol element. Thus, while the results are obtained for the single set of composite parameters given in table 2, the topology of the resonance surfaces for arbitrary composite geometries will be equivalent to those presented in this paper, but scaled along the input power axis.

The magnitude of the resonance tunability and the effect of the bias magnetic field on the surfaces will be altered if the Galfenol properties given in table 2 are modified. The material anisotropy constants, K^k, and saturation magnetization, M_s, have a minimal effect on Galfenol's elastic modulus behavior shown in figure 5. However, the averaging factor Ω (which accounts for material imperfections) and the magnetostriction constant λ_{100} directly control the ΔE effect. Referring to figure 1, the smoothness of the transition between the two linear elastic branches is controlled by Ω, while λ_{100} controls the width of the transition. As such, the ΔE effect is enhanced as the magnetostriction constant increases and as the amount of material imperfections (Ω) decreases. Only small improvements over the Ω value of 776.73 used in this paper can be expected, as evidenced by the reported values of Ω for Galfenol in the literature (500 to 2100 [14, 16, 23]). A λ_{100} value of 157×10^{-6} is used in this paper, yielding $E_0 = 28.6$ GPa. From (1), this results in $\Delta E_{max} \approx 100\%$. If the maximum λ_{100} value for polycrystalline Galfenol—187×10^{-6} [3]—is instead used, then $E_0 = 23.5$ GPa and $\Delta E_{max} \approx 150\%$. Therefore, the resonance tunability results presented in this paper are relatively conservative estimations of the true potential of Galfenol-based active composites.

The effect of the boundary conditions on the natural frequency surfaces is small for both parametric studies. The thresholds of the input power amplitude are lower for the C–F boundary condition due to the composite's increased compliance, as discussed above. As seen in figures 12 and 15, the boundary condition has an insignificant effect on the maximum resonance tunability in all cases. For the C–C beam, as the magnetic field increases a compressive blocking stress develops to constrain the Galfenol element and prevent magnetostriction along the axis of the beam. It is well known that this will result in an effective softening of the beam with respect to transverse vibration, and will thus contribute to the resonance tuning response of the vibration absorber. This effect is not included in the proposed model and should be investigated in future studies.

6. Conclusions

This paper investigated the semi-active control of a magnetically-tunable vibration absorber's resonance frequency. The vibration absorber that was considered is a metal-matrix composite containing the magnetostrictive material Galfenol with an aluminum matrix. For computational purposes, the composite was modeled as a single degree of freedom system. The complex constitutive behavior was included by using a fully nonlinear, anhysteretic model of Galfenol from the literature. Despite the one-dimensional simplification, the variation in Galfenol's elastic modulus along the length and through the thickness of the Galfenol element was retained by considering the stress distribution throughout the element and the asymmetric tension–compression behavior of Galfenol. Two boundary conditions—cantilevered and clamped–clamped—were imposed on the composite. Resonance tunability of the absorber was investigated by computing its frequency response to harmonic base excitation as a function of the operating conditions—input power amplitude and bias magnetic field. Parametric studies were presented to characterize the effect on resonance tunability of Galfenol volume fraction and Galfenol's location within the composite.

Results and conclusions from the study are summarized as follows.

- Nearly uniform controllability of the vibration absorber's resonance frequency is possible below a threshold of the input power amplitude. The resonance frequency is modulated between its minimum and maximum using weak magnetic fields of 0 to 8 kA m^{-1}. As the input power amplitude increases above the threshold, the controllability decreases and stronger magnetic fields are required to realize the control.
- The boundary condition imposed on the composite was found to have a minimal effect on its resonance tuning behavior. However, the model does not include the effect of axial loading, which is well known to affect the resonance frequency of transverse vibration in beams.

- When the Galfenol element is located at the neutral axis, the maximum resonance tunability varies between 2.5% and 49% as Galfenol volume fraction increases from 10% to 100%.
- When Galfenol volume fraction is fixed at 10%, the maximum resonance tunability varies between 2.5% and 5.5% as the Galfenol element is offset from the composite's midplane.
- It was reasoned that the resonance tuning results presented in this paper are conservative estimates of the true potential of Galfenol-based vibration absorbers, and can be applied to systems with differences in composite geometry and certain Galfenol material properties.

Acknowledgments

This work was supported by a Graduate Automotive Technology Education (GATE) Fellowship from the US DOE GATE Center of Excellence, DE FG2605NT42616, at The Ohio State University. Additional support was provided by the member organizations of the Smart Vehicle Concepts Center (www.SmartVehicleCenter.org), a National Science Foundation Industry/University Cooperative Research Center (I/UCRC). This work was supported in part by an allocation of computing time from the Ohio Supercomputer Center.

Appendix. Galfenol constitutive model (ED model)

In this model, energy expressions are derived to describe the rotation of each magnetically easy crystal direction, or direction in which the material prefers to magnetize, resulting from application of stress $\mathbf{T}$ and magnetic field $\mathbf{H}$. Table A.1 summarizes the energy terms for the kth magnetic domain orientation [14], where $\mathbf{c}^k$ are the magnetically easy crystal directions in the zero stress and zero magnetic field state, K^k and K_0^k are material anisotropy constants, M_s is the saturation magnetization for the material, and μ_0 is the magnetic permeability of free space.

The total free energy G^k is represented in matrix form as

$$G^k = \tfrac{1}{2}\mathbf{m}^k \cdot \mathbf{K}^k \mathbf{m}^k - \mathbf{m}^k \cdot \mathbf{B}^k + \tfrac{1}{2}K^k + K_0^k, \qquad \text{(A.1)}$$

where the magnetic stiffness matrix $\mathbf{K}^k$ and force vector $\mathbf{B}^k$ are

$$\mathbf{K}^k = \begin{bmatrix} K^k - 3\lambda_{100}T_1 & -3\lambda_{111}T_4 & -3\lambda_{111}T_6 \\ -3\lambda_{111}T_4 & K^k - 3\lambda_{100}T_2 & -3\lambda_{111}T_5 \\ -3\lambda_{111}T_6 & -3\lambda_{111}T_5 & K^k - 3\lambda_{100}T_3 \end{bmatrix}, \qquad \text{(A.2)}$$

$$\mathbf{B}^k = \begin{bmatrix} c_1^k K^k + \mu_0 M_s H_1 & c_2^k K^k + \mu_0 M_s H_2 & c_3^k K^k + \mu_0 M_s H_3 \end{bmatrix}^{\mathrm{T}}, \qquad \text{(A.3)}$$

Table A.1. Energies of the magnetic domain orientations in the ED model.

Anisotropy	Magnetomechanical coupling	Zeeman (magnetic field)
$\frac{1}{2}K^k\lvert\mathbf{m}^k - \mathbf{c}^k\rvert^2 + K_0^k$	$-\mathbf{S}_m^k \cdot \mathbf{T}$	$-\mu_0 M_s \mathbf{m}^k \cdot \mathbf{H}$

and λ_{100} and λ_{111} are magnetostriction constants. Magnetic domain orientations $\mathbf{m}^k$ are calculated by minimizing each energy expression while constraining $\mathbf{m}^k$ to have unity norm, resulting in

$$\mathbf{m}^k = (\mathbf{K}^k)^{-1}\left[\mathbf{B}^k + \frac{1 - \mathbf{c}^k \cdot (\mathbf{K}^k)^{-1}\mathbf{B}^k}{\mathbf{c}^k \cdot (\mathbf{K}^k)^{-1}\mathbf{c}^k}\mathbf{c}^k\right]. \qquad \text{(A.4)}$$

The anhysteretic volume fractions ξ_{an}^k of idealized magnetic domains oriented along each of the easy directions is then calculated by an energy-weighted average,

$$\xi_{an}^k = \frac{\exp(-G^k/\Omega)}{\sum_{k=1}^{r}\exp(-G^k/\Omega)}, \qquad \text{(A.5)}$$

where Ω is the experimentally-derived averaging factor to account for material defects, and r is the number of easy crystal directions, which depends upon crystal symmetry. Finally, bulk magnetization $\mathbf{M}$ and magnetostriction $\mathbf{S}_m$ are calculated as the sum of the contribution from each orientation (i.e., $M_s\mathbf{m}^k$) weighted by the volume fraction of domains in each orientation ξ_{an}^k,

$$\mathbf{M} = M_s \sum_{k=1}^{r} \xi_{an}^k \mathbf{m}^k, \qquad \mathbf{S}_m = \sum_{k=1}^{r} \xi_{an}^k \mathbf{S}_m^k. \qquad \text{(A.6)}$$

The bulk strain $\mathbf{S}$ is then calculated as the sum of magnetostriction and mechanical strain.

References

[1] Rustighi E, Brennan M J and Mace B R 2004 A shape memory alloy adaptive tuned vibration absorber: design and implementation *Smart Mater. Struct.* **14** 19

[2] Atulasimha J and Flatau A B 2011 A review of magnetostrictive iron–gallium alloys *Smart Mater. Struct.* **20** 043001

[3] Jones N J, Restorff J B, Wun-Fogle M and Clark A E 2010 Magnetostriction and magnetization of tension annealed rods of $Fe_{82}Ga_{18}$ *J. Appl. Phys.* **107** 09A915

[4] Datta S and Flatau A B 2008 Magnetomechanical coupling factor and energy density of single crystal iron–gallium alloys *Proc. SPIE* **6929** 69291Z

[5] Etrema Products, Inc. 2013 *Terfenol-D Data Sheet* available online

[6] Wilkie W K, Inman D J, Lloyd J M and High J W 2006 Anisotropic laminar piezocomposite actuator incorporating machined PMN–PT single-crystal fibers *J. Intell. Mater. Syst. Struct.* **17** 15–28

[7] Bozorth R M 1951 *Ferromagnetism* D Van Nostrand Co. Inc, Princeton, NJ

[8] Flatau A B, Dapino M J and Calkins F T 2000 High bandwidth tunability in a smart vibration absorber *J. Intell. Mater. Syst. Struct.* **11** 923–9

[9] Schick D, Babu S S, Foster D R, Dapino M, Short M and Lippold J C 2011 Transient thermal response in ultrasonic additive manufacturing of aluminum 3003 *Rapid Prototyping J.* **17** 369–79

[10] Mudivarthi C, Datta S, Atulasimha J and Flatau A B 2008 A bidirectionally coupled magnetoelastic model and its validation using a Galfenol unimorph sensor *Smart Mater. Struct.* **17** 035005

[11] Braghin F, Cinquemani S and Resta F 2011 A model of magnetostrictive actuators for active vibration control *Sensors Actuators* A **165** 342–50

[12] Shu L, Dapino M J, Evans P G, Chen D and Lu Q 2011 Optimization and dynamic modeling of Galfenol unimorphs *J. Intell. Mater. Syst. Struct.* **22** 781–93
[13] Zhou H M and Zhou Y H 2007 Vibration suppression of laminated composite beams using actuators of giant magnetostrictive materials *Smart Mater. Struct.* **16** 198
[14] Evans P G and Dapino M J 2010 Efficient magnetic hysteresis model for field and stress application in magnetostrictive Galfenol *J. Appl. Phys.* **107** 063906
[15] Scheidler J J and Dapino M J 2013 Nonlinear dynamic model for magnetically-tunable Galfenol vibration absorbers *Proc. SPIE* **8690** 869002
[16] Chakrabarti S 2011 Modeling of 3D magnetostrictive systems with application to Galfenol and Terfenol-D transducers *PhD Thesis* The Ohio State University
[17] Chakrabarti S and Dapino M J 2011 Nonlinear finite element model for 3D Galfenol systems *Smart Mater. Struct.* **20** 105034
[18] Evans P G and Dapino M J 2011 Dynamic model for 3D magnetostrictive transducers *IEEE Trans. Magn.* **47** 221–30
[19] Deng Z and Dapino M J 2013 Characterization and finite element modeling of Galfenol minor flux density loops *Proc. SPIE* **8689** 86890V
[20] Weng L, Walker T, Deng Z, Dapino M J and Wang B 2013 Major and minor stress–magnetization loops in textured polycrystalline $Fe_{81.6}Ga_{18.4}$ Galfenol *J. Appl. Phys.* **113** 024508
[21] Meirovitch L 2010 *Fundamentals of Vibrations* 1st edn (Long Grove, IL: Waveland Press)
[22] Staab G H 1999 *Laminar Composites* (Boston, MA: Butterworth–Heinemann)
[23] Atulasimha J, Flatau A B and Summers E 2007 Characterization and energy-based model of the magnetomechanical behavior of polycrystalline iron–gallium alloys *Smart Mater. Struct.* **16** 1265